UNIVERSITY OF CALIFORNIA SAN DIEGO

Design and Manipulation of On-Chip Bragg Couplers for Side Lobe Suppression

A thesis submission in partial satisfaction of the requirements for the degree of Master of Sciences

in

Electrical Engineering (Photonics)

by

Sushant Kumar

Committee in charge:

Professor Yeshaiahu Fainman, Chair

Professor Vitaliy Lomakin

Professor George Papen

2018

The Thesis of Sushant Kumar is approved, and it is acceptable in quality and form for publication on microfilm and electronically:

Chair

University of California San Diego

2018

Dedication

This thesis and research work is dedicated to my parents and sister without whose support I would not be where I am today. What we are is accumulation of all life experiences and hence; I would also like to recognize my friends, fellow lab-mates and all the instructors through my educational career.

Epigraph

Many things which nature makes difficult become easy to the man who uses his brains.

Hannibal Barca

The scientific man does not aim at an immediate result. He does not expect that his advanced ideas will be readily taken up. His work is like that of the planter – for the future. His duty is to lay the foundation for those who are to come, and point the way.

Nikola Tesla

Table of Contents

List of Figures

Acknowledgements

This work was done under the mentorship of Professor Yeshaiahu Fainman (Chair) and with constant guidance from Dr. Andrew Grieco. I would also like to acknowledge the assistance of Jordan Davis with regards to simulations in LUMERICAL.

Chapter 1 may be used in part or full for future publications. The author of this thesis will be the principal author of said publications, co-authored by A. Grieco and Y. Fainman.

Chapter 2 may be used in part or full for future publications. The author of this thesis will be the principal author of said publications, co-authored by A. Grieco and Y. Fainman.

Chapter may be used in part or full for future publications. The author of this thesis will be the principal author of said publications, co-authored by A. Grieco and Y. Fainman.

Chapter 4 may be used in part or full for future publications. The author of this thesis will be the principal author of said publications, co-authored by A. Grieco and Y. Fainman.

Chapter 5 may be used in part or full for future publications. The author of this thesis will be the principal author of said publications, co-authored by A. Grieco and Y. Fainman.

ABSTRACT OF THE THESIS

Design and Manipulation of On-Chip Bragg Couplers for Side Lobe Suppression

by

Sushant Kumar

Master of Sciences in Electrical Engineering (Photonics)

University of California San Diego, 2018

Professor Yeshaiahu Fainman, Chair

Contra-directional Bragg couplers are an integral part of many present and future on-chip optical systems. Suppression of side lobes of such filters is important for near and long term practical applications of optical devices in

multiple disciplines. This thesis investigates the apodization of Bragg devices for side lobe suppression and points out some flaws in the design approach. Post numerical analysis, a method of cascaded coupler design is developed. Through numerical simulations, it is demonstrated that the cascaded coupler approach is a superior method for maintaining spectral purity of the coupled optical signal. A roadmap for device design to withstand fabrication errors and make the device tunable is also suggested.

Introduction and Motivation

Optical devices are becoming a mainstay in various applications ranging from communications to mobile spectroscopy etc. Considering the ever-increasing need for bandwidth leading to the requirement for better signal to noise ratio (SNR), lo signal crosstalk. faster modulation speeds and mass production potential; silicon photonic devices appear to be the most logical way forward. Silicon devices offer high index contrast leading to better confinement and smaller device sizes; in addition to being compatible with the Complementary Metal Oxide Semiconductor (CMOS) foundry processes, which would allow for leveraging of the billions of dollars already invested on the electronics side of the industry. Contra-directional Bragg couplers offer broadband and tunable solution for multidisciplinary applications in the field of photonics. But, in order to achieve a high SNR and low crosstalk in the coupled optical fields the side lobes of the coupling spectra of the Bragg devices need to be suppressed.

Apodization of contra-directional Bragg couplers is the most prevalent method of accomplishing this goal. But, this approach acts only to smoothen the spectrum of the Bragg device and doesn’t actually filter out power from the side lobes. As such I may in fact increase the crosstalk between closely spaced channels or channel groups. This may prove to be problematic in case of dense

wavelength division multiplexing (DWDM) or on chip laser-based applications, where spectral purity and low channel crosstalk are of utmost importance.

Hence, a better design for side lobe suppression of contra-directional Bragg couplers is needed. Considering this a point of departure, the method of cascaded Bragg couplers is presented as a solution in this thesis. Chapter 1 contains a theoretical description of inter-modal coupling via Bragg devices. This chapter contains a derivation of the coupled mode theory starting from Maxwell's equations. Chapter 2 furthers Chapter 1, by providing analytical and numerical analysis of the coupled mode equations of the contra-directional two-port Bragg devices. The viability of transfer matrix method to obtain solutions to coupled mode equations is also discussed. Chapter 3 presents numerical analysis of four-port Bragg coupler devices via transfer matrix method. This chapter also discusses apodized contra-directional Bragg devices and points out the points of failure of such designs. Chapter 4 describes the method of cascaded Bragg devices for the purpose of side-lobe suppression. In this chapter, full FDTD simulations of these devices are presented. Chapter 5 contains a quick comparison of the two approaches and points out advantages and disadvantages of the cascaded device method versus the apodization method. Chapter 6 points to the future roadmap for design and fabrication of the cascaded contra-directional Bragg coupler devices.

1. Theory of Bragg Couplers

1.1 Maxwell's Equations

The mathematical and physical theory of any Bragg device begins with Maxwell's equations that describe the electromagnetic fields in any medium. The equations (Eqs.) are general knowledge in scientific community [1] [2]and are as follows:

$$\nabla \cdot \boldsymbol{D} = \rho \ , \tag{1.1}$$

$$\nabla \times \boldsymbol{H} - \frac{\partial \boldsymbol{D}}{\partial t} = \boldsymbol{J} \ , \tag{1.2}$$

$$\nabla \times \boldsymbol{E} + \frac{\partial \boldsymbol{B}}{\partial t} = 0 \ , \tag{1.3}$$

$$\nabla \cdot \boldsymbol{B} = 0 \ , \tag{1.4}$$

Where $\boldsymbol{E}$ and $\boldsymbol{H}$ are vector electric and magnetic fields. $\boldsymbol{D}$ and $\boldsymbol{B}$ are electric displacement and magnetic induction fields vectors, while $\boldsymbol{\rho}$ is electric charge

density and $\boldsymbol{J}$ is the electric current density. In any material $\boldsymbol{D}$ and $\boldsymbol{B}$ can be related to the $\boldsymbol{E}$ and $\boldsymbol{H}$ fields using the following equations:

$$\boldsymbol{E} = \varepsilon \boldsymbol{E} = \varepsilon_0 \boldsymbol{E} + \boldsymbol{P} \quad (1.5)$$

$$\boldsymbol{B} = \mu \boldsymbol{H} = u_0 \boldsymbol{H} + \boldsymbol{M} \quad (1.6)$$

Where $\boldsymbol{P}$ is electric polarization and $\boldsymbol{M}$ is magnetization. These are material properties and can be real or complex and range from zero in case of non-electronic and magnetic materials; to positive or negative. These properties can be in tensor form to model more nuanced material properties such as non-linearities, hysteresis etc.

1.2 Source and Divergence Free Maxwell's Equations

If simple CMOS martials like Silicon and Silicon Oxide with almost non-existent anisotropy and non-linearity are in consideration. The ε and μ can be taken as scalar constants and the impressed charge densities ρ and impressed current $\boldsymbol{J}$ densities are negligible. Provided the above conditions are met; a simplified version of electromagnetic wave equations can be obtained by applying the curl operator to Eqs. (1.2) and (1.3) to get:

$$\nabla \times (\nabla \times \boldsymbol{H}) + \varepsilon \frac{\partial}{\partial t}(\nabla \times \boldsymbol{E}) = 0$$

(1.7)

$$\nabla \times (\nabla \times \boldsymbol{E}) + \mu \frac{\partial}{\partial t}(\nabla \times \boldsymbol{H}) = 0\,,$$

(1.8)

Then, Eqs. (1.3) and (1.2) can be substituted into Eqs. (1.7) and (1.8) to separate the variables and get:

$$\nabla \times (\nabla \times \boldsymbol{H}) + \mu\varepsilon \frac{\partial^2 \boldsymbol{H}}{\partial t^2} = 0$$

(1.9)

$$\nabla \times (\nabla \times \boldsymbol{E}) + \mu\varepsilon \frac{\partial^2 \boldsymbol{E}}{\partial t^2} = 0$$

(1.10)

Utilizing the following vector identity:

$$\nabla \times (\nabla \times \boldsymbol{A}) = \nabla(\nabla \cdot \boldsymbol{A}) - \nabla^2 \boldsymbol{A}$$

(1.11)

And also observing that Eqs. (1.1) and (1.4) equate to zero due to almost non-existent source charges and currents in the material; the divergence free vector equations can be obtained:

$$\nabla^2 \boldsymbol{H} = u\varepsilon \frac{\partial^2 \boldsymbol{H}}{\partial t^2} = \frac{n^2}{c^2} \frac{\partial^2 \boldsymbol{H}}{\partial t^2} \tag{1.12}$$

$$\nabla^2 \boldsymbol{E} = u\varepsilon \frac{\partial^2 \boldsymbol{E}}{\partial t^2} = \frac{n^2}{c^2} \frac{\partial^2 \boldsymbol{E}}{\partial t^2} \tag{1.13}$$

$$c = {1}\Big/{\sqrt{\varepsilon_0 \mu_0}} \tag{1.14}$$

$$n = {\sqrt{\varepsilon \mu}}\Big/{\sqrt{\varepsilon_0 \mu_0}} \tag{1.15}$$

Here, c is the speed of light in vacuum and n is the refractive index of the material (Silicon or Silicon Oxide for the purpose of this thesis).

In bulk material, Eqs. (1.12) and (1.13) result in plane wave solutions for Cartesian coordinate systems. Presence of additional boundary conditions; like a waveguide wherein a Silicon core is surrounded by Silicon Oxide. The solutions represent guided modes with a propagation constant β . Sine the devices in consideration are planar in nature, the materials can be considered to be homogeneous in z-direction for the coupled mode theory considerations. In this case, permittivity and permeability can assume the form:

$$\varepsilon(x, y, z, t) = \varepsilon(x, y) \tag{1.16}$$

$$\mu(x, y, z, t) = \mu(x, y) \tag{1.17}$$

Where x, y and z are cartesian coordinates while t is the time coordinate. When Eqs. (1.16) and (1.17) are applied to the Maxwell's wave equations (1.12) and (1.13). The solutions of the wave equations become of the form:

$$\boldsymbol{H}(x, y, z, t) = Re\{\boldsymbol{H_m}(y, z)\, exp[i(\omega t - \beta_m x)]\} \tag{1.18}$$

$$\boldsymbol{E}(x, y, z, t) = Re\{\boldsymbol{E_m}(y, z)\, exp[i(\omega t - \beta_m x)]\}$$

(1.19)

Where ω is the angular frequency of the optical field, the subscript m signifies the m^{th} mode of the waveguide and β_m refers to the propagation constant of the m^{th} mode along x; which is the direction of propagation in this case. In most cases the modes subscripts are discrete due to the quantized nature of guided modes in slab or in this case, strip waveguides. It is pertinent to know that analytical solutions to the wave equations are known for multiple geometries and boundary conditions. But, in most cases; the solutions are computed numerically using any of the various computer software at hand.

1.3 Orthonormalization of Electromagnetic Modes

For systems where permittivity and permeability are invariant along the direction of propagation, it can be demonstrated that modes of the form of Eqs. (2.18) and (2.19) are orthogonal in nature. This can be done by considering the spatial characteristics of the electromagnetic fields. Since the modes are eigenvalue solutions, to the Maxwell's wave equations; they must be invariant along direction of propagation given non-existent field-loss and invariant

permittivity and permeability profiles. If multiple modes are excited in a system, the total electric and magnetic fields present in the system can be described by:

$$\boldsymbol{E}(x,y,z,t) = Re\left\{\sum_{\boldsymbol{m}} \boldsymbol{E_m}\,(y,z)\,exp[i(\omega t - \beta_m x)]\right\} \tag{1.20}$$

$$\boldsymbol{H}(x,y,z,t) = Re\left\{\sum_{\boldsymbol{m}} \boldsymbol{H_m}\,(y,z)\,exp[i(\omega t - \beta_m x)]\right\} \tag{1.21}$$

Time averaged power is defined as:

$$\boldsymbol{P} = \int\int [\boldsymbol{E}(x,y,z,t)] \times [\boldsymbol{H}(x,y,z,t)]^*\ dy\,dz \tag{1.22}$$

Replacing (1.20) and (1.21) into (1.22), we can get time averaged power; since the conjugate in the $\boldsymbol{H}$ field cancels out the exponential term in the expression of $\boldsymbol{P}$. Leading to a time averaged value of power.

$$\boldsymbol{P} = \iint_{-\infty}^{-\infty} \frac{1}{2} Re\left\{\left[\sum_m \boldsymbol{E_n}(y,z)\,exp(-i\beta_m x)\right] \times \left[\sum_n \boldsymbol{H_n^*}(y,z)\,exp(i\beta_n x)\right] \cdot \boldsymbol{n_x}\right\} dy\,dz$$

$$\boldsymbol{P} = \frac{1}{2} Re \left\{ \sum_{m} \sum_{n} exp[i(\beta_n - \beta_m)] \iint_{-\infty}^{\infty} \boldsymbol{E_m}(y,z) \times \boldsymbol{H_n^*}(y,z) \cdot \boldsymbol{n_x}\, dy\, dz \right\}$$

(1.23)

Where $\boldsymbol{n_x}$ is unit vector along the direction of propagation x. Considering the condition of continuous and constant power-flow, equation (1.23) becomes:

$$0 = \frac{\partial \boldsymbol{P}}{\partial x} = \frac{1}{2} Re \left\{ \sum_{m} \sum_{n} exp[i(\beta_n - \beta_m)] \iint_{-\infty}^{\infty} \boldsymbol{E_m}(y,z) \times \boldsymbol{H_n^*}(y,z) \cdot \boldsymbol{n_x}\, dy\, dz \right\}$$

(1.24)

Upon close inspection it is evident that power in each mode is continuous, leading to the following orthonormalization condition for the fields:

$$\left| \frac{1}{2} Re \left\{ \iint_{-\infty}^{\infty} \boldsymbol{E_m}(y,z) \times \boldsymbol{H_n^*}(y,z) \cdot \boldsymbol{n_x}\, dy\, dz \right\} \right| = \delta_{mn}$$

(1.25)

where δ_{mn} is the Kronecker delta i.e. the integral is non-zero only if $m = n$.

The Kronecker delta is taken to have the units of power and modes are normalized to unity. The absolute value is included because the sign of power-flow depends on the direction of propagation.

From the above relation of electromagnetic power-flow, additional information with regards to constrains between electric and magnetic fields can be derived. Similar to decoupling of electric and magnetic fields shown in Eqs. (1.9) and (1.10), the equality in power-flow can be expressed as:

$$\frac{1}{2}\,\varepsilon|\boldsymbol{E}|^2 = \frac{1}{2}\,\mu|\boldsymbol{H}|^2 \tag{1.26}$$

The full derivation for the above expression can be found in references [1] [2].

It should be kept in mind, that the above energy and power-flow equalities are valid only if the permittivity and permeability distributions are homogeneous and their gradient is negligible. The orthonormalization condition is a direct result of the modal solutions to Maxwell's equations and the fact that modal energy may only be scaled by any factor for all modes together and not individual modes. Since, the energy may be normalized arbitrarily; either the electric or magnetic fields can be normalized to unity.

1.4 Lorentz Reciprocity Theorem

The most general approach to electromagnetic mode coupling in general relies on the well-known *Lorentz Reciprocity Theorem* [3]. The theorem is derived by considering arbitrary solutions to Maxwell's equations for a pair of distinct waveguides with distinct modes. The electric and magnetic fields in the individual modes in source-free, non-magnetic dielectric media can be denoted by $\boldsymbol{E_1}, \boldsymbol{H_1}$ and $\boldsymbol{E_2}, \boldsymbol{H_2}$ respectively. Solving the Maxwell's Eqs (1.2) and (1.3).

$$\nabla \times \boldsymbol{H_1} = i\omega\varepsilon \boldsymbol{E_1} \ ,$$

$$\nabla \times \boldsymbol{E_1} = -i\omega\mu \boldsymbol{H_1}$$

(1.27)

$$\nabla \times \boldsymbol{H_2} = i\omega\varepsilon \boldsymbol{E_2} \ ,$$

$$\nabla \times \boldsymbol{E_2} = -i\omega\mu \boldsymbol{H_2}$$

(1.28)

Applying the following vector identity to the above Eqs.:

$$\nabla \cdot (\boldsymbol{A} \times \boldsymbol{B}) = \boldsymbol{B} \cdot (\nabla \times \boldsymbol{A}) - \boldsymbol{A} \cdot (\nabla \times \boldsymbol{B})$$

(1.29)

We get the following equation pairs:

$$\nabla \cdot (\boldsymbol{E_1^*} \times \boldsymbol{H_2}) = \boldsymbol{H_2} \cdot \nabla \times \boldsymbol{E_1^*} - \boldsymbol{E_1^*} \cdot \nabla \times \boldsymbol{H_2} = \boldsymbol{H_2} \cdot i\omega \boldsymbol{H_1^*} + \boldsymbol{E_1^*} \cdot i\omega \varepsilon_2 \boldsymbol{E_2}$$

$$\nabla \cdot (\boldsymbol{E_2} \times \boldsymbol{H_1^*}) = \boldsymbol{H_1^*} \cdot \nabla \times \boldsymbol{E_2} - \boldsymbol{E_2} \cdot \nabla \times \boldsymbol{H_1^*} = \boldsymbol{H_1^*} \cdot i\omega \boldsymbol{H_2} + \boldsymbol{E_2} \cdot i\omega \varepsilon_1 \boldsymbol{E_1^*}$$

(1.30)

The addition of the above pair leads to Lorentz Reciprocity theorem:

$$\nabla \cdot (\boldsymbol{E_1^*} \times \boldsymbol{H_2}) + \nabla \cdot (\boldsymbol{E_2} \times \boldsymbol{H_1^*}) = -i\omega(\varepsilon_2 - \varepsilon_1)\boldsymbol{E_1^*} \cdot \boldsymbol{E_2}$$

(1.31)

The above is applicable not only for differing sets of permittivity but also different sets or permeability or any combination of these material properties. Application of Lorentz Reciprocity in the case of waveguides, requires integration on each side of Eq. (1.31) over an arbitrary volume and application of Gauss' theorem as follows:

$$\iiint_V \nabla \cdot \boldsymbol{\phi}\, dV = \iint_s \boldsymbol{\phi} \cdot ds$$

(1.32)

Where V and S are the desired volume and surface of integration. The application of (1.32) on (1.31) leads to:

$$\iint_{\nabla S} (\boldsymbol{E_1^*} \times \boldsymbol{H_2^*} + \boldsymbol{E_2} \times \boldsymbol{H_2^*}) \cdot ds = -i\omega \iiint_{V} (\varepsilon_2 - \varepsilon_1) \boldsymbol{E_1^*} \cdot \boldsymbol{E_2}\, dV$$

(1.33)

Considering the case of guided modes and utilizing the knowledge that in transverse direction, the integration is taken at infinity such that all the power in all possible modes is taken into account and the integral in the direction of propagation is infinitesimally small. Considering x to be the direction of propagation, the guided modes vanish far away from the waveguide core; since the fields decay exponentially away from the core and the integral reduces to:

$$\iint_{S} \frac{\partial}{\partial x} (\boldsymbol{E_1^*} \times \boldsymbol{H_2^*} + \boldsymbol{E_2} \times \boldsymbol{H_2^*}) \cdot dS = -i\omega \iint_{S} (\varepsilon_2 - \varepsilon_1) \boldsymbol{E_1^*} \cdot \boldsymbol{E_2}\, dS$$

(1.34)

Form the above set of equations, coupled mode equations can be derived. This is done in the proceeding section.

1.5 Coupled Mode Theory

The modes described by (1.20) and (1.21) form a complete basis set, such that any arbitrary field can be expressed as:

$$\boldsymbol{E}(x,y,z,t) = Re\left\{\sum_{\boldsymbol{m}} A_m \boldsymbol{E_m}(y,z)\, exp[i(\omega t - \beta_m x)]\right\}$$

(1.35)

$$\boldsymbol{H}(x,y,z,t) = Re\left\{\sum_{\boldsymbol{m}} A_m \boldsymbol{H_m}(y,z)\, exp[i(\omega t - \beta_m x)]\right\}$$

(1.36)

Where A_m is a constant term reflecting the weight of each basis mode and the mode coefficient m is summed over all mode indices. In the propagation media, if a perturbation of permittivity $\Delta\varepsilon$ such that:

$$\varepsilon(x,y,z) = \varepsilon(y,z) + \Delta\varepsilon(x,y,z)$$

(1.37)

In the preceding formulation, where no perturbation was present the fields could be expressed purely in terms of unperturbed modes where the mode weights A_m were invariant in the direction of propagation. In presence of perturbed permittivity in the direction of propagation, the modes can still be expressed in terms of unperturbed modal basis. However, since the eigenmode basis of the perturbed region are not the same as those of the unperturbed region; the

weighting coefficients A_m must become dependent in the direction of propagation x.

$$\boldsymbol{E}(x,y,z,t) = Re\left\{\sum_{\boldsymbol{m}} A_m(x)\boldsymbol{E_m}\,(y,z)\,exp[i(\omega t - \beta_m x)]\right\}$$

(1.38)

$$\boldsymbol{H}(x,y,z,t) = Re\left\{\sum_{\boldsymbol{m}} A_m(x)\boldsymbol{H_m}\,(y,z)\,exp[i(\omega t - \beta_m x)]\right\}$$

(1.39)

Due to the nature of derivation, Eqs. (1.38) and (1.39) still follow Maxwell's equations. The coupled mode equations can be derived by applying Lorentz Reciprocity to Eqs. (1.38) and (1.39), which produces:

$$\sum_m \left[i(\beta_n - \beta_m)A_m(x) + \frac{dA_m(x)}{dx}\right] exp[i(\beta_n - \beta_m)x] \iint (\boldsymbol{E_n^*} \times \boldsymbol{H_m} + \boldsymbol{E_m} \times \boldsymbol{H_n^*}) \cdot n_x \, dy \; dz$$

$$= \sum_m [-i\omega A_m(x)]\, exp[i(\beta_n - \beta_m)x] \iint \Delta\varepsilon(\boldsymbol{E_m^*} \cdot \boldsymbol{E_n^*})\, dy \; dz$$

(1.40)

The above expressions were derived by associating the perturbed and unperturbed modal decompositions and utilizing the assumption that the perturbation is small enough such that the change in the basis weighting coefficients $A_m(x)$ is almost non-existent between the perturbed and unperturbed regions. It should be kept in mind, that coupled mode equations in general are valid even if the perturbations aren't small. Appropriate expressions can be derived from original Maxwell's equations for larger perturbations provided the above approximation is not made while deriving the expressions.

The expression for electric fields can be further simplified using the normalization condition (1.25), to obtain:

$$\frac{dA_n(x)}{dx} = \sum_m \frac{i\omega}{2} A_m(x) \exp[i(\beta_n - \beta_m)x] \frac{\int\int \Delta\varepsilon(\boldsymbol{E_m^*}\cdot\boldsymbol{E_n^*})\, dy\ dz}{\int\int \boldsymbol{E_n}\times\boldsymbol{H_n^*}\cdot\boldsymbol{n_x}\, dy\, dz} \tag{1.41}$$

The above expression provides us with a differential equation describing the coupling of power between two sets of modes indexed by m and n respectively. In simple words, the above expression describes coupling between one set of modes with another set of modes due to small perturbations in permittivity. It should be noted that similar expressions can be obtained for small perturbations in permeability or the for magnetic fields.

1.6 Modal Coupling in Bragg Devices

Bragg devices achieve coupling of power between otherwise orthogonal modes via periodic perturbation. Conveniently, for a periodic perturbation in x direction; the permittivity can be decomposed into a Fourier series, resulting in:

$$\Delta\varepsilon(x,y,z) = \sum_{l} \varepsilon_l(y,z)\, exp\left(-il\frac{2\pi x}{\Lambda}\right) - i\delta \tag{1.42}$$

Where Λ is the period of the perturbation, l indicates the order of the Fourier series term in consideration and δ accounts for almost all physical sources of losses in a waveguide. Substituting this Fourier series into the coupled mode Eqs. (1.41), the following expression can be obtained:

$$\frac{dA_n(x)}{dz} = \frac{\beta_n\alpha_n}{2|\beta_n|}A_n(x) - i\frac{\beta_n}{|\beta_n|}\sum_{l}\sum_{m} k_{lnm}A_m(x)\exp[i\left(\beta_n - \beta_m - l\frac{2\pi x}{\Lambda}\right)x] \tag{1.43}$$

$$k_{lnm} = \frac{\omega\iint \varepsilon_l(y,z)(\boldsymbol{E_m^*}\cdot\boldsymbol{E_n^*})\,dy\;dz}{2\iint \varepsilon(\boldsymbol{E_m^*}\cdot\boldsymbol{H_n^*})\,dy\;dz} \tag{1.44}$$

Where k_{lnm} describes the strength of coupling between the n^{th} mode and the m^{th} mode due to l^{th} Fourier term. The coefficient α_n represent the linear power loss of the n^{th} mode as it propagates in the waveguide. These losses account not only due to the imaginary part of the propagation constant, but also due to any other physical phenomena. It should be noted that the coupled mode equations take different forms depending on the direction of propagation, this is made clear by the ratio of the propagation constant to its magnitude. Given the nature of the phenomenon, every mode interacts with every other mode. But, over a long length of interaction between the any pair of modes; in case of phase mismatch the exponential term washes out the exchange of power. Therefore, significant power is exchanged between any pair of modes only when the modes are phase matched. That is, the term in the exponential present in the coupled mode equation (1.43) goes to zero:

$$\beta_n - \beta_m - l\frac{2\pi x}{\Lambda} = 0 \tag{1.45}$$

So, the periodicity of the perturbation determines which modes interact strongly; leading to a significant exchange of power between the said pair of modes.

Acknowledgement:

This chapter may be used in part or full for future publications. The author of this thesis will be the principal author of said publications, co-authored by A. Grieco and Y. Fainman.

2. Two-Port Bragg Devices

2.1 Coupled Mode Analysis of Two-Port Bragg Devices

The phenomenon of coupling between contra directional modes can be most simply demonstrated in two-port Bragg device. Such devices are most commonly used as integrated mirrors or band-rejection filters in on-chip and fiber optic applications. But, anti-reflection coatings operate on the same exact theoretical basis and are possibly the most prevalent application utilizing Bragg reflection phenomena.

In general, such devices can be modelled using the first order coupling coefficients calculated using the first order Fourier series term. It is the case, because the second order terms are minimal in magnitude and lead to insignificant coupling over the length of the device and lead to only second order errors in theoretical calculations, which can be easily ignored in these devices. Also, the following calculations considering lossless modes, that is; the loss coefficients α_n corresponding to each mode are considered to be negligible and hence are ignored.

Considering a waveguide, the coupling between a forward propagating mode (denoted by the subscript f) and a backward propagating mode (denoted

by the subscript b) arising from the first order coupling coefficient can be described using the following coupled mode equations [1]:

$$\frac{dA_n(x)}{dx} = -ik_{fb}A_b(x)e^{i\Delta\beta x} \tag{2.1}$$

$$\frac{dA_b(x)}{dx} = ik_{bf}A_b(x)e^{1i\Delta\beta x} \tag{2.2}$$

$$\beta_f - (-\beta_b) - l\frac{2\pi x}{\Lambda} = \Delta\beta \tag{2.3}$$

In the above expressions, $l = 1$ since only the first order Fourier coefficients are taken into account, but this can be done for any number of Fourier orders. It should also be kept in mind that the following relation exists between the coupling coefficients:

$$k_{bf} = k_{fb}^{*} \tag{2.4}$$

Which is a consequence of the definition of coupling coefficients between a pair of modes (1.44) and the relationship between Fourier coefficients (1.42). The

above pair of equations can be solved utilizing standard method for eigen-value problems.

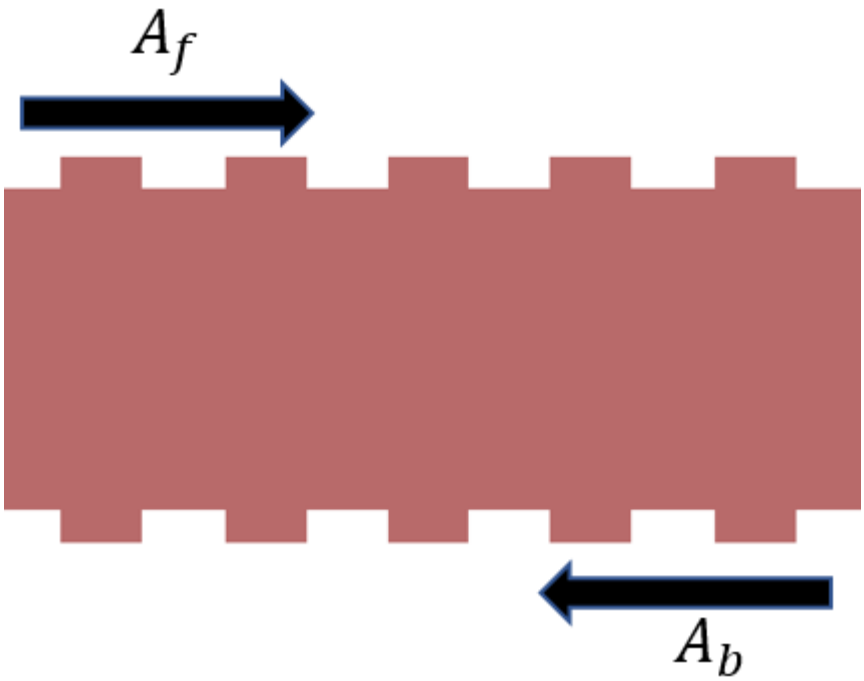

Figure 2.1: A typical Two-port Bragg device. The arrows indicate the amplitudes of the forward and backward propagating modes.

Taking the above approach, the amplitudes of the forward and backward propagating modes can be assumed to have the general expression as follows:

$$A_f(x) = exp\left(\frac{j\Delta\beta x}{2}\right)[C_1\, exp(sx) + C_2\, exp(-sx)] \tag{2.5}$$

$$A_b(x) = exp\left(\frac{-j\Delta\beta x}{2}\right)[D_1\, exp(sx) + D_2\, exp(-sx)]$$

(2.6)

$$s = \sqrt{k_{fb}k_{bf} - \left(\frac{\Delta\beta}{2}\right)^2}$$

(2.7)

Where C_1, C_2, D_1 and D_2 are constants determined by initial condition of the fields.

If forward propagating field is considered to be the input. Then it can be normalized to unity and every other field every other field can be derived as a fraction of that. If the above case is applied, the following boundary conditions can be imposed:

$$A_f(0) = 1$$

(2.8)

$$A_b(L) = 0$$

(2.9)

Where L is the length of the Bragg device. Applying Eqs. (2.5), (2.6) in addition to the boundary conditions (2.8) and (2.9) to the coupled mode equations (2.1) and (2.2) result in:

$$C_1 = \frac{\left(s - \frac{i\Delta B}{2}\right) exp(-sx)}{i\Delta\beta\, sinh(sL) + 2s\, cosh(sL)} \tag{2.10}$$

$$D_1 = \frac{ik_{fb}\, exp(-sL)}{i\Delta\beta\, sinh(sL) + 2s\, cosh(sL)} \tag{2.11}$$

The values of reflection amplitude r_{fb} and transmission amplitude t_{fb} can be determined by combining the coefficients as solutions to the coupled mode equations.

$$r_{fb} = \frac{A_b(0)}{A_f(0)} = \frac{-2ik_{fb}\, sin\, h(sL)}{i\Delta\beta\, sinh(sL) + 2s\, cosh(sL)} \tag{2.12}$$

$$t_{ff} = \frac{A_f(L)}{A_f(0)} = \frac{2s\ exp\left(\frac{j\Delta\beta L}{2}\right)}{i\Delta\beta_{sinh}(sL) + 2s\ cosh(sL)}$$

(2.13)

2.2 Transfer Matrix Analysis of Two-Port Bragg Devices

The set of coupled mode equations describing two-port Bragg devices {Eqs. (2.1) and (2.2)} can also be numerically analyzed using transfer matrix formalism [4], [5]. This can be done by representing the coupled mode equations in the form:

$$\dot{E}(x) = A\,E(x) \;\rightarrow E(x) = T(x\,,\,x_0)E(x_0)$$

(2.14)

$$E(x) = \begin{bmatrix} A_f(x) \\ A_b(x) \end{bmatrix}$$

(2.15)

$$T(x\,,\,x_0) = \; e^{S_1(x\,-x_0)}e^{S_1(x\,-x_0)}$$

(2.16)

$$S_1(x - x_0) = \begin{pmatrix} j\Delta\beta & 0 \\ 0 & -j\Delta\beta \end{pmatrix}$$

(2.14)

$$S_2(x - x_0) = \begin{pmatrix} -j\Delta\beta_2 & 0 \\ 0 & j\Delta\beta_2 \end{pmatrix}$$

(2.14)

The above approach is valid only for small perturbations, since the coupled mode equations that lead to the above matrices are themselves limited by the assumption of small perturbation in permittivity or permeability.

This approach is very convenient for numerical calculations and simulations due to its matrix approach, allowing for easier discretization in the real space or frequency domain. The use of matrices also simplifies numerical simulation of more complicated structures like, a resonant cavity formed by cascading multiple two-port devices [6]. The matrix equation (2.14) was solved using MATLAB.

2.3 Results

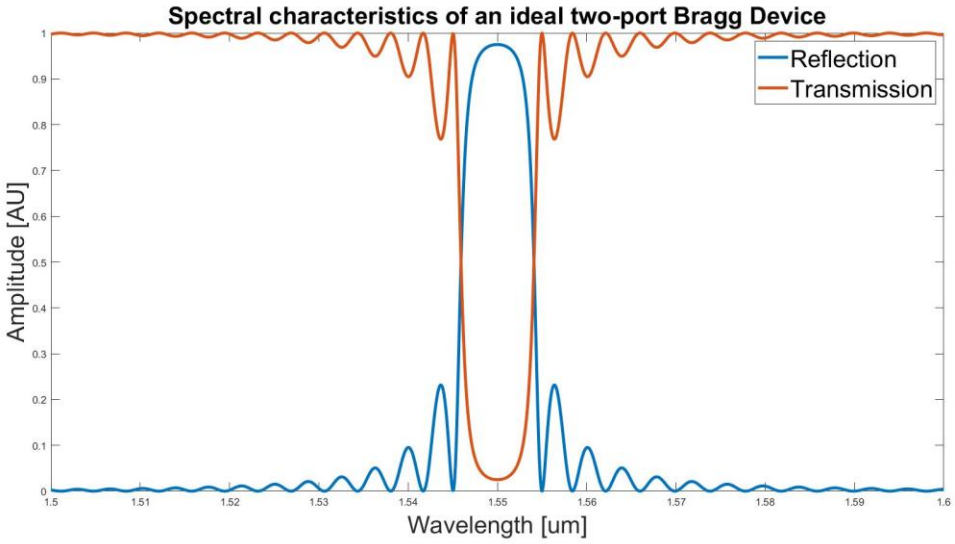

Figure 2.2: Spectral characteristic of a typical Two-port Bragg device.

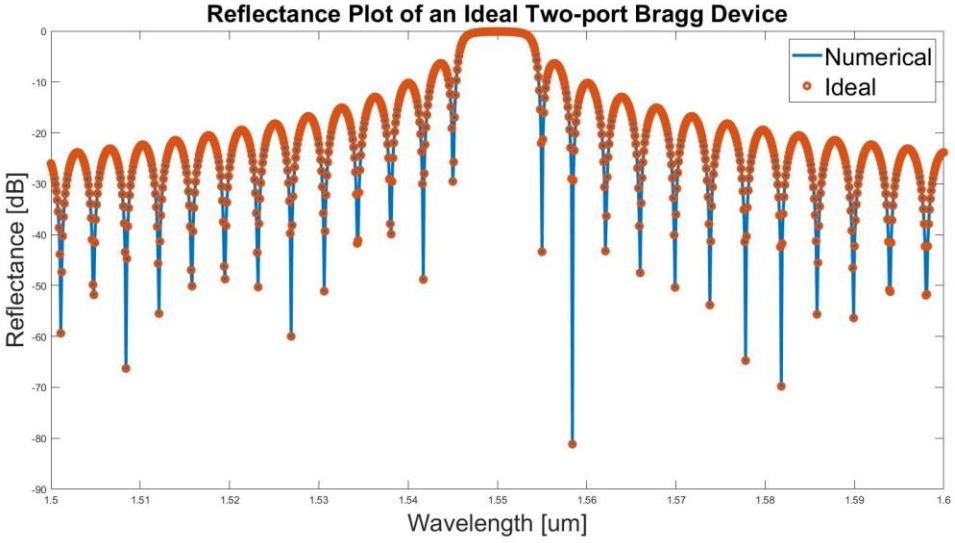

Figure 2.3: Comparison of the analytical and numerical (Transfer Matrix) analysis of the Spectral characteristic of a typical Two-port Bragg device.

Figure 2.2 demonstrates a typical spectral response of a lossless two-port Bragg device. It should be noted that the power in both modes always adds up to unity at all frequencies. This is what makes the device lossless.

For Figure 2.3 a four hundred period two-port Bragg device was numerically simulated in MATLAB using transfer matrix approach and compared to the frequency response obtained from the above derived expression (2.12). As can be seen, both the transfer matrix and the analytical approach lead to results that match exactly. This reinforces the eligibility of transfer matrix approach for coupled mode analysis of more complicated systems, which tend to be have very cumbersome analytical solutions. It should also be noted that if the coupling coefficients are purely real then the inclusion of conjugate doesn't have any effect on Eqs. (2.4). This is a very plausible case in lossless considerations, and as such; from this point on, all the coupling coefficients are considered purely real.

Ideally, flat side-bands are desired in the spectral response of a mirror or a band-pass filter. But, Bragg devices are not ideal for such application even when they are lossless. As seen in Figures 2.2 & 2.3, they tend to have side-lobes that can be very significant at times. Methods for suppression of these undesired characteristics are discussed in Chapter 3 and 4.

Acknowledgement:

This chapter may be used in part or full for future publications. The author of this thesis will be the principal author of said publications, co-authored by A. Grieco and Y. Fainman.

3. Four-Port Bragg Devices and Apodization

Four-port Bragg devices are very commonly used for coupling of power between dissimilar waveguides. Co-directional waveguide couplers and ring resonator couplers are the two other most common approaches to coupling power between waveguides. But, co-directional waveguide couplers suffer from sensitivity towards the frequency composition of the input signal and the length of coupling. The cyclic nature of energy exchange over the interaction length and its dependence on frequency almost make co-directional waveguide couplers monochromatic in design and highly susceptible to fabrication errors. Ring resonator couplers on the other hand, are robust to fabrication errors to some degree, but display either high degree of losses or very small Free Spectral Range (FSR). If the ring resonators are designed for big FSR, they show high losses due to small turn radius leading to power leaking into undesired modes and slab modes. However, if low losses are desired, the rings can be designed with large turning radii. In that case, they end up with a very small FSR and offer very little to no wavelength selectivity.

The control over location of the coupled spectrum via control pf the periodicity, in addition to the frequency specific nature of the design give Bragg-couplers and advantage over co-directional waveguide couplers and ring resonator couplers. Thus, thorough understanding of Bragg-couplers for future development of integrated optics is important.

3.1 Transfer Matrix Analysis of Four-Port Bragg Devices

Four-port Bragg devices can be visualized as a pair of dissimilar waveguides, such that their unperturbed modes are not phase matched and hence no significant coupling happens in absence of perturbation.

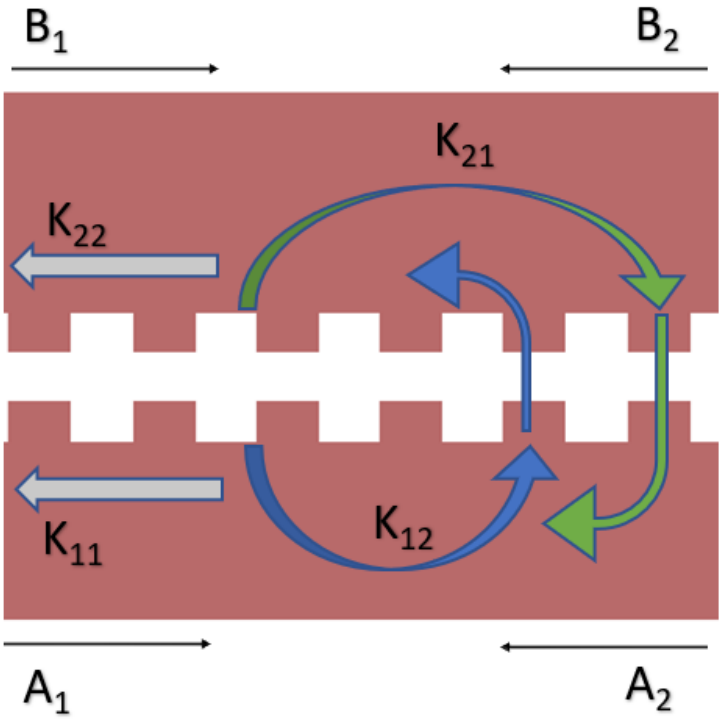

Figure 3.1: A typical Four-port Bragg coupler.

The system can be seen as having pairs of forward and backward propagating modes in each of the waveguides. Hence, the system can be described using the following coupled mode formulation[4], [5], [6]:

$$\frac{dA_1}{dx} = -jk_{11}A_2e^{j2\Delta\beta_1 x} - jk_{21}B_2e^{j(\Delta\beta_1+\Delta\beta_2)x}$$

(3.1)

$$\frac{dB_1}{dx} = -jk_{12}A_2e^{j(\Delta\beta_1+\Delta\beta_2)x} - jk_{22}B_2e^{j2\Delta\beta_2 x}$$

(3.2)

$$\frac{dA_2}{dx} = jk_{11}^*A_1e^{-j2\Delta\beta_1 x} + jk_{12}^*B_1e^{-j(\Delta\beta_1+\Delta\beta_2)x}$$

(3.3)

$$\frac{dB_1}{dx} = jk_{12}^*A_1e^{-j(\Delta\beta_1+\Delta\beta_2)x} + jk_{22}^*B_1e^{-j2\Delta\beta_2 x}$$

(3.4)

Where A_1 & B_1 are forward propagating modes in each waveguide, while A_2 & B_2 are backward propagating modes. As seen in (1.44), the strength of coupling between a pair of modes is determined by the overlap of the fields from the modes in consideration and the value of the Fourier coefficient being accounted for. The modes must also be phase matched (1.45) for the exchange of power to take place. The above equations present a significant challenge in

terms of analysis. But, the above Eqs. (3.1 – 3.4) can also be presented in the transfer matrix formulation:

$$\dot{E}(x) = A\,E(x) \;\rightarrow E(x) = T(x\,,\,x_0)E(x_0)$$

(3.5)

where

$$E(x) = \begin{bmatrix} A_1(x) \\ B_1(x) \\ A_2(x) \\ B_2(x) \end{bmatrix} \qquad T(x\,,\,x_0) = \; e^{S_1(x\,-x_0)}e^{S_1(x\,-x_0)}$$

(3.6) (3.7)

And

$$S_1(x - x_0) = \begin{pmatrix} j\Delta\beta_1 & 0 & 0 & 0 \\ 0 & j\Delta\beta_2 & 0 & 0 \\ 0 & 0 & -j\Delta\beta_1 & 0 \\ 0 & 0 & 0 & -j\Delta\beta_2 \end{pmatrix}$$

(3.8)

$$S_1(x - x_0) =$$

$$\begin{pmatrix} -j\Delta\beta_1 & 0 & -jk_{11}e^{j2\Delta\beta_1(x-x_0)} & -jk_{12}e^{j(\Delta\beta_1+\Delta\beta_2)(x-x_0)} \\ 0 & -j\Delta\beta_2 & -jk_{12}e^{j(\Delta\beta_1+\Delta\beta_2)(x-x_0)} & -jk_{22}e^{j2\Delta\beta_2(x-x_0)} \\ jk_{11}e^{-j2\Delta\beta_1\,(x-x_0)} & jk_{12}e^{-j(\Delta\beta_1+\Delta\beta_2)(x-x_0)} & j\Delta\beta_1 & 0 \\ jk_{12}e^{-j(\Delta\beta_1+\Delta\beta_2)(x-x_0)} & jk_{12}e^{-j\Delta\beta_2(x-x_0)} & 0 & j\Delta\beta_2 \end{pmatrix}$$

(3.9)

The above matrix equation was solved using MATLAB for devices with six hundred periods and periodicity such that the forward propagating mode from the first waveguide (A_1) is phase matched with the backward propagating mode (B_2) in the second waveguide. Since the spectrum for Bragg devices are symmetric about the central wavelength, only one half of the spectrum was simulated to minimize computation time. It should also be noted, that all the coupling coefficients taken into consideration were purely real and hence the conjugate from 2.4 was excluded from the coupled mode and transfer matrix formulations. In case the coupling coefficients are not purely real, the system can still be modelled using transfer matrix formulation, since the underlying equations place no constraints on the values that the coupling coefficients can take.

As expected, due to the nature of the underlying theory and formulation. The contra directional coupling spectrum for a four-port Bragg device looks very much like the coupling spectrum for a two-port device (Figure: 2.3).

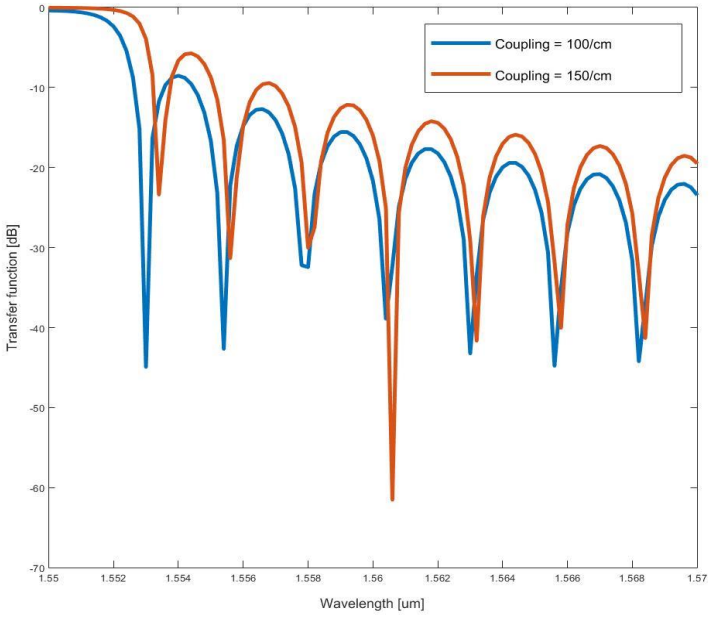

Figure 3.2: Spectra of Four-port Bragg couplers with different coupling coefficients.

It should be noted that, for a simple four-port Bragg coupler, the main-lobe and side-lobe differ by almost -6dB in magnitude. Another point worth observing is that, a change in coupling coefficient leads to a noticeable change in the location of the minima for the main-lobe and the subsequent side-lobes. Physically, it means that a Bragg coupler with stronger coupling characteristics like; being closely spaced or more significant perturbations will have a more broadband response when compared to a device with weaker coupling characteristics [7].

3.2 Apodized Bragg Devices

As hinted in section 2.3, power in side-lobes is an undesirable characteristic for many applications of Bragg devices. Power in side lobe can be seen as undesired signal in spectroscopy or camera system applications and as cross-talk in optical communication applications. Therefore, removal of power from side-lobes can be considered an important improvement in the vanilla Bragg-coupler design.

The most prevalent approach for side-lobe suppression in Bragg couplers is the apodization of coupling coefficient profile along the length of the coupler. Apodization has its origin and most wide-spread usage in Digital Signal Processing (DSP), Diffractive Optics and later on Antennae Systems. In DSP, apodized time windows are used to avoid the high frequencies generated but the traditional square window. In diffractive optics, the aperture for a camera lens or any other optical element is apodized to avoid spatial side lobes and improve the Signal to Noise Ratio (SNR). Similarly, an antennae system uses apodization to improve the directionality of the antennae and improves its SNR and cross-talk. Even in the field of integrated optics, apodized Arrayed Waveguide Gratings (AWG) are a very common application of apodization for improvement in directionality of the structure.

For on-chip Bragg couplers, apodization is achieved through variation in coupling coefficient profile along the length of the coupler. This can be achieved

either by varying the amount of perturbation along the length of the coupler or by altering the spacing between the two waveguides. Both approaches are effective and produce similar results.

Analysis of apodized Bragg devices can be done using the coupled mode and transfer matrix formalisms used in section 3.1. For the purpose of demonstration, a Bragg device with six hundred periods was simulated using MATLAB. To model apodization, the structure was discretized into sections with a certain number of periods. Each section had a constant coupling coefficient, but the coupling coefficient for each section was varied as a function of x to account for apodization.

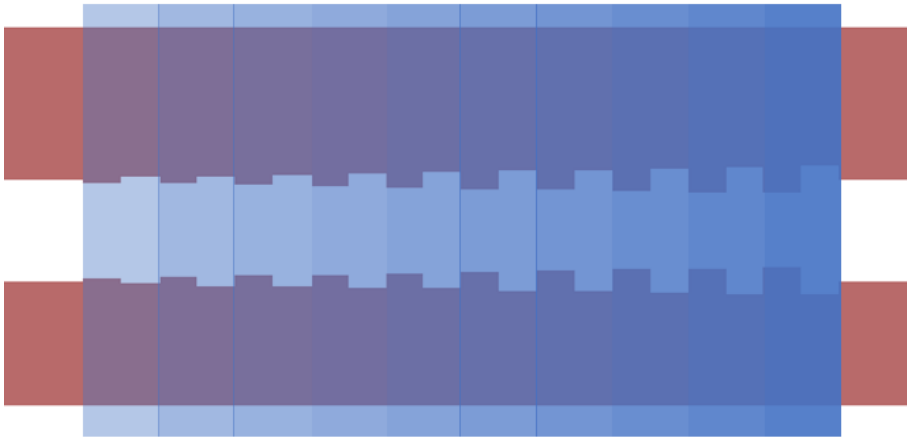

Figure 3.3: A linearly apodized Four-port Bragg coupler. The transparency indicates the strength of coupling in the region.

A linear apodization profile was chosen to demonstrate the effects of anodization in Bragg devices. Devices with five and ten discretized sections with different apodization slopes were simulated.

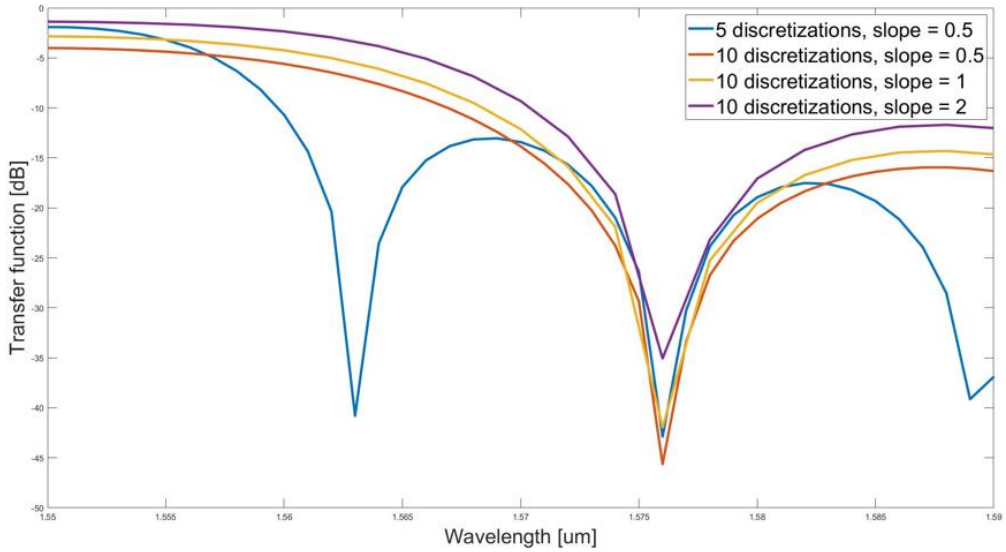

Figure 3.4: Spectra for linearly apodized Four-port Bragg coupler. The different discretizations and slopes are shown in different colours.

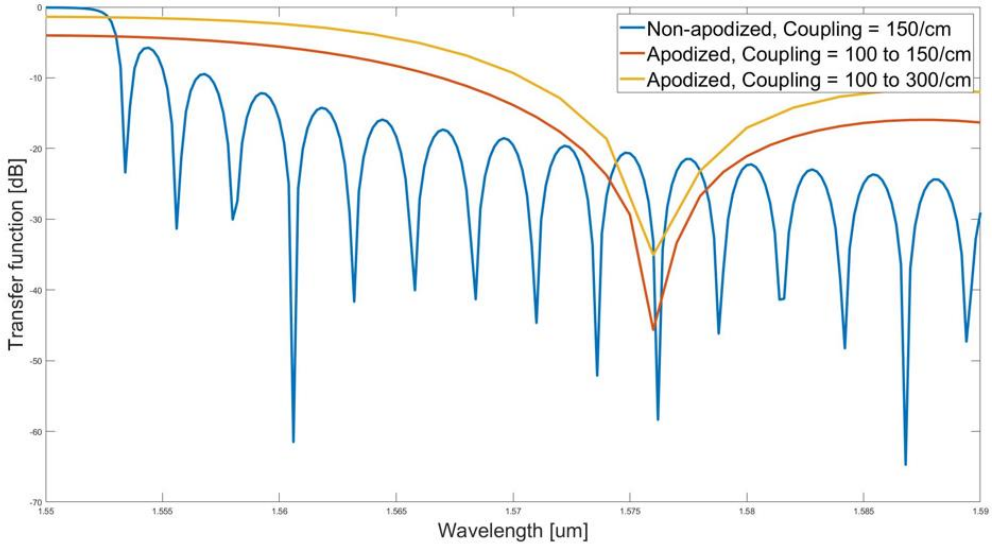

Figure 3.5: Spectra for linearly apodized Four-port Bragg couplers with and without apodization. Both discretized devices had ten discretized sections.

It can be seen (Figure 3.4) that more discretized, filters display the effects of apodization more prominently; since the filter with five discrete sections has a spectrum more similar to a vanilla four-port Bragg device than a device with ten discrete sections. Also, it is to be noted that the slope of the apodization scheme has very little effect on the location of the side bands, but it does affect the amount of power coupled into the contra-directional mode, as evident from the difference in main lobe height in Figures 3.4 and 3.5.

Lastly and most importantly, it should be noted that apodization scheme shown here doesn't actually filter out power from undesired frequencies (that is, the side-lobes). Apodization decidedly broadens the main lobe and smoothens out the spectrum, so that it appears as if the side lobes are suppressed, but in reality; the side lobes just become a part of the main lobe. Consequently, more power ends up being coupled into the undesired (side-lobe) frequencies than the original filter design. The results, although surprising are not entirely new. Similar results were obtained in a previous publication [8] based on purely theoretical and numerical analysis. It should also be noted that similar results were obtained by [9] even though, the device was carefully designed, simulated and fabricated. The device in [9] uses weakly coupled waveguides and Gaussian apodization profile. It is by far, one of the best specimens of apodized Bragg couplers. And yet, it suffers from the same issue of more power being coupled into the side-lobe due to broadening of the main lobe. Therefore, apodization although very prevalent; is not a suitable approach for suppression of side lobes.

Acknowledgement:

This chapter may be used in part or full for future publications. The author of this thesis will be the principal author of said publications, co-authored by A. Grieco and Y. Fainman.

4. Cascaded Bragg Couplers

As shown in Chapter 3, apodization is not an effective method for elimination of power from undesired frequencies in the spectral response of a Bragg device. Considering the utility of contra-directional Bragg couplers in current and future integrated optical devices; a new approach for filtration of power from side lobes is needed. The approach of Cascaded Bragg Couplers takes advantage of the fact that the relative width of the min lobe can be tuned depending on the strength of coupling between the modes in consideration.

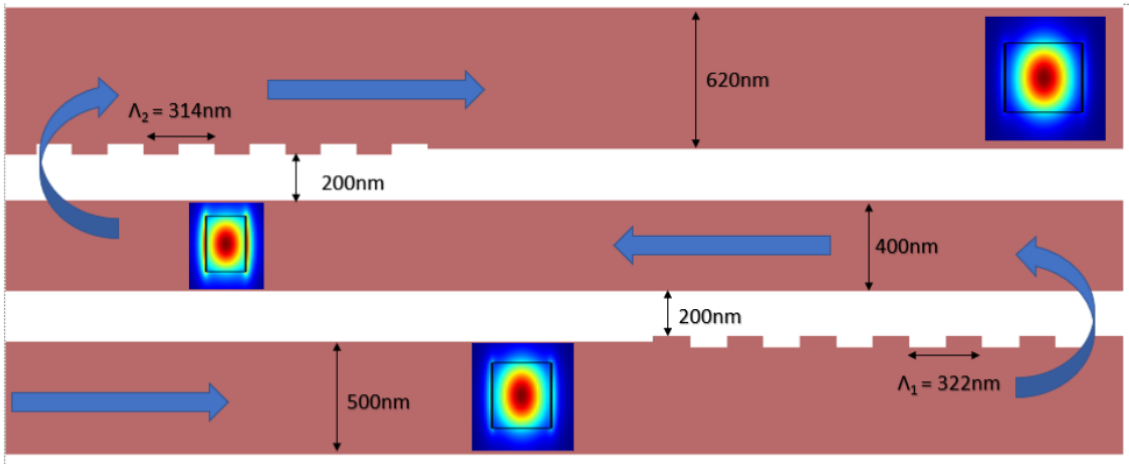

Figure 4.1: Design of cascaded Bragg Devices. Relative electric field intensities of fundamental TE_0 modes for each waveguide are shown.

The filters were designed using three dissimilar 220nm thick Silicon waveguides, clad with SiO_2 all around. Both the 500nm and 600nm waveguides had 50nm perturbations. It is plenty evident from the modal profiles of the fundamental TE_0 modes (Figure 4.1) for each waveguide that, the mode in the

wider (600nm) waveguide is better confined that the mode in the narrower waveguide (500nm). Since both waveguides interact with the 400nm intermediary waveguide and have 50nm perturbations. Due to difference in modal overlap, the coupling strength for the 500nm – 400nm waveguide pair is stronger; than the coupling strength between the 400nm – 600nm pair.

In cascading the Bragg couplers, the spectra of individual filters are tuned such that the first filter has a broader main lobe than the second filter. But, the design is done such that the minima of the main lobe from the first device is as close as possible to the maxima of the side lobes from the spectrum of the second device. This ensures that there is very little power at the frequencies where the side lobes of the second filter couple power. Ideally, if the minima of the first filter can be matched exactly with the maxima of the side lobes for the second filter, minimum possible power will be coupled into the side lobes at the final output.

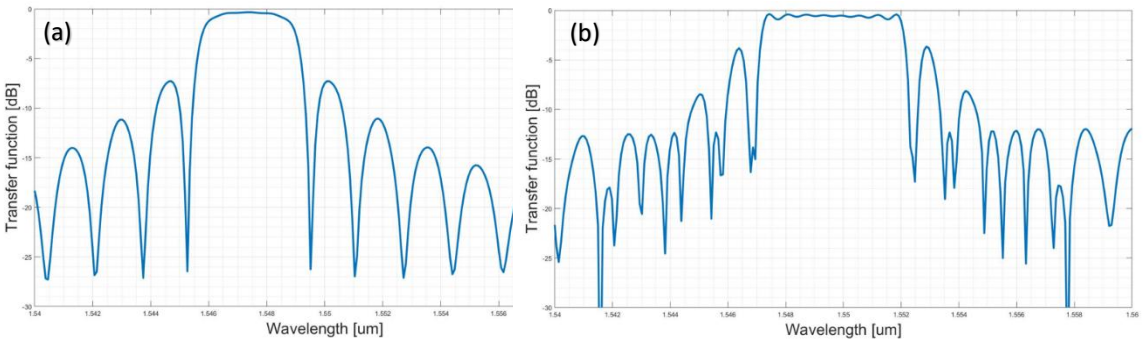

Figure 4.2: Spectrum of a single Bragg couplers (a) 400nm – 600nm waveguide pair; (b) 500nm – 400nm waveguide pair.

The cascaded filter design was simulated in LUMERICAL using FDTD method. As can be seen from the FDTD spectrum of the 400nm - 600nm pair versus 500nm – 400nm pair. The main lobe is wider for the 500nm – 400nm pair and the side lobes are higher indicating stronger coupling. It should be noted that (Figure 4.2 - a & b) for single stage Bragg devices, the side lobes are -6.5dB and -4.5dB lower than the main lobe for the 400nm – 600nm and 500nm – 400nm pair respectively.

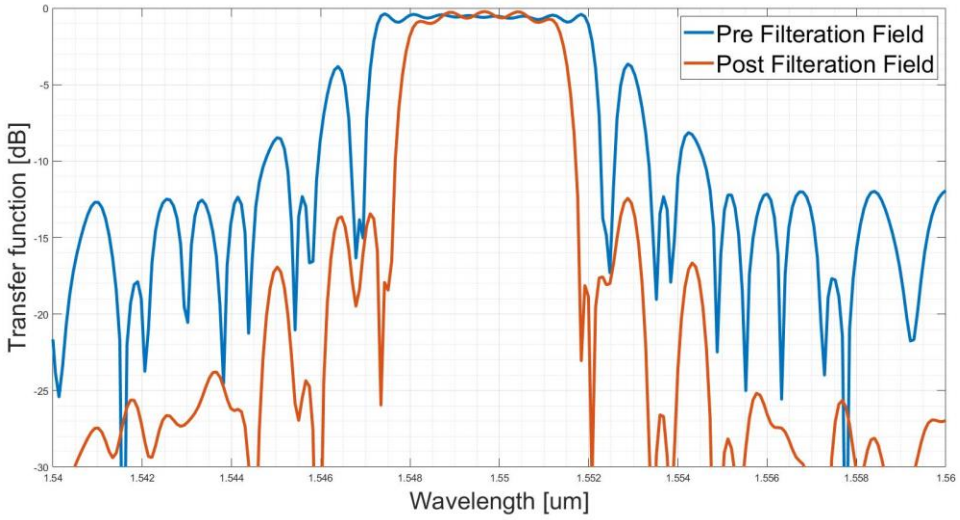

Figure 4.3: Spectrum of the device pre-second stage filtering (blue) and post second stage filtering (orange).

As evidenced from Figure 4.3, the side lobe is -12.5dB as compared to the best case -6.5dB (Figure 4.2-a). This is possible because by cascading the Bragg couplers, power is removed from the side-lobe regions. Therefore, the side lobes for the second stage have less than unity power to couple from while the main lobe can have power close to unit if the devices are long enough.

Acknowledgement:

This chapter may be used in part or full for future publications. The author of this thesis will be the principal author of said publications, co-authored by A. Grieco and Y. Fainman.

5. Conclusion and Roadmap

Chapter 4 provides evidence that while the concept of apodization is widely used, it doesn't actually serve its purpose. It merely smoothens out the spectrum of the Bragg coupler while actually accentuating the power in the side lobes. Even state of the art apodized Bragg devices with very long interaction length and very weak coupling [9] don't manage to filter out the power present in side lobes. It can be speculated that the application of apodization schemes in the case of Bragg devices doesn't fit in the context of frequency filtering. In all other examples of apodized systems, there is a direct mapping between the domains of interest. In DSP the domains of time and frequency can be easily mapped using Fourier transformations. Similarly, in the fields of antennae and Arrayed Waveguide Gratings, the grating profile is manipulated in real space to get desired results in the Fourier space (since spatial frequencies are altered, leading to more directionality). Again, the two domains of interest can be easily mapped using Fourier transformations. But, in the application of Bragg couplers for frequency filtering; the device's profile is altered in real space while observing results in frequency space. The two domains may not be linearly mapped with each other leading to the effects observed in case of apodization of Bragg couplers.

The cascaded Bragg device approach shows significantly between suppression of side lobe. The device design provides the frequency selectivity

and low loss properties of regular Bragg grating devices while also avoiding the natural pitfalls of the vanilla design. The cascaded coupler approach is also more resistant to fabrication errors than the apodization scheme. Since both waveguide pairs have 50nm perturbation, in case of fabrication error, the perturbations in both pairs will be affected in similar fashion and percentage. Since, the critical point of this approach depends on the widths of the main-lobes for each pair. As long as both sets of waveguide pairs are affected in same fashion, the design should be able to function as intended.

The second point of emphasis for the cascaded filter approach is the selection of periodicity for the two filters.

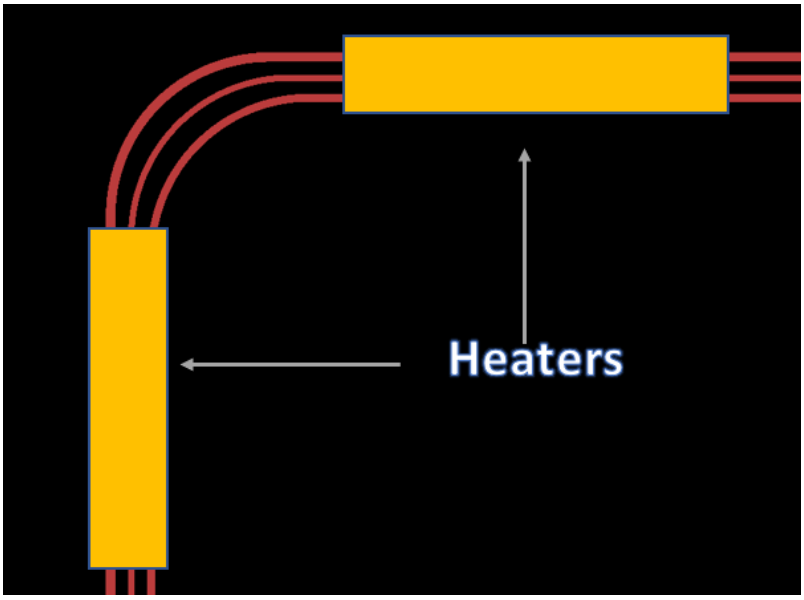

Figure 5.1: Design for fabrication of the cascaded filter scheme.

The device is under fabrication at the NANO3 facility at UCSD. In case of fabrication errors and mismatch of periodicities of the two filters, heaters can be deposited on top of each pair. The change in temperature generates carriers in Si leading to a change in permittivity in the affected regions. The change in permittivity can shift the central wavelength of the main lobe. So, in case of fabrication errors, the heaters provide another avenue for adjustment; making the design more resistant. It should also be noted that in Figure 5.1, each of the filter sections are placed away from each other so as to minimize the thermal coupling between them; in case differential thermal tuning is required.

It should also be noted that in this case the filters were designed for fundamental TE_{00} modes. But, such Bragg devices can also be used for higher order modes as well [6]. Another point of development in the design would be for coupling between lower to higher order modes.

Acknowledgement:

This chapter may be used in part or full for future publications. The author of this thesis will be the principal author of said publications, co-authored by A. Grieco and Y. Fainman.

References

[1] A. Yariv and P. Yeh, “Optical Waves in Crystals,” Hoboken, NJ: John Wiley and Sons, 2003.

[2] J. M. Jin, “Theory and Computation of Electromagnetic Fields,” Wiley-IEEE, Second Edition.

[3] H. Kogelnik, "2. Theory of Dielectric Waveguides," in Integrated Optics (Topics in Applied Physics), Berlin, DE, Springer-Verlag, 1975, pp. 13-81.

[4] Weber J.P. , “Spectral Characteristics of Coupled-waveguide Bragg-reflection tunable optical filter,” IEEE Proceedings J-Vol.140(5), Oct 1993.

[5] Wei Shi, Xu Wang, Charlie Lin, Han Yun, Yang Liu, Tom Baehr-Jones, Michael Hochberg, Nicolas A. F. Jaeger, and Lukas Chrostowski, "Silicon photonic grating-assisted, contra-directional couplers," Opt. Express 21, 3633-3650 (2013).

[6] J. A. Davis, A. Grieco, M. C. M. M. Souza, N. C. Frateschi, and Y. Fainman, "Hybrid multimode resonators based on grating-assisted counter-directional couplers," Opt. Express 25, 16484-16490 (2017)

[7] A. Grieco, B. Slutsky and Y. Fainman, “Characterization of waveguide loss using distributed Bragg reflectors,” Applied Physics B, Vol.114, Springer, 2014.

[8] Kogelink H., “Filter Response of Nonuniform Almost-Periodic Structures,” Bell Systems Technical Journal V. 55(1), Jan 1976.

[9] Shi, W., Yun, H., Lin, C., Flueckiger, J., Jaeger, N. A. F., & Chrostowski, L. (2013). “Coupler-apodized Bragg-grating add – drop filter,” *38*(16), 3068–3070.